CLM-R217

CLM-R217

UKAEA

Report

SOME INITIAL CONSIDERATIONS ON THE SUITABILITY OF FERRITIC/MARTENSITIC STAINLESS STEELS AS FIRST WALL AND BLANKET MATERIALS IN FUSION REACTORS

G. J. BUTTERWORTH

CULHAM LABORATORY
Abingdon Oxfordshire

1982

C18 Available from H. M. Stationery Office £2.00

SOME INITIAL CONSIDERATIONS ON THE SUITABILITY OF FERRITIC/MARTENSITIC STAINLESS STEELS AS FIRST WALL AND BLANKET MATERIALS IN FUSION REACTORS

G.J. Butterworth

Culham Laboratory, Abingdon, Oxon, OX14 3DB, UK

(Euratom/UKAEA Fusion Association)

Abstract

Iron-based stainless steel alloys are among the principal candidate materials for the first wall/blanket components of nuclear fusion reactors. Recent evidence from irradiation tests in fission reactors suggests that martensitic/ferritic alloys may offer a significant increase in lifetime in comparison with the austenitic grades currently favoured. The first part of this paper briefly describes the constitution of stainless iron alloys and discusses the characteristic properties of alloys in the main ferritic, martensitic and austenitic groups on the basis of their structural and compositional differences. A comparison of published data on the mechanical, thermal and irradiation properties of typical austenitic and martensitic/ferritic steels shows that alloys in the latter groups have certain advantages for fusion applications. The ferromagnetism exhibited by martensitic and ferritic alloys has, however, been identified as a potentially serious obstacle to their utilisation in magnetic confinement devices. The paper describes measurements performed in other laboratories on the magnetic properties of two representative martensitic alloys 12Cr-1Mo and 9Cr-2Mo. These observations show that a modest bias magnetic field of magnitude 1 - 2 tesla induces a state of magnetic saturation in these materials. They would thus behave as essentially paramagnetic materials having a relative permeability close to unity when saturated by the toroidal field of a tokamak reactor. The results of computations by the General Atomic research group to assess the implications of such magnetic behaviour on reactor design and operation are presented. The results so far indicate that the ferromagnetism of martensitic/ferritic steels would not represent a major obstacle to their utilisation as first wall or blanket materials.

August 1981

ISBN 0 85311 098 0

CONTENTS

1. INTRODUCTION

The first wall and blanket structure in a fusion reactor fulfils a number of functions. Firstly, it serves as a membrane isolating the coolant at a pressure up to 50 bar from the low pressure deuterium and tritium fuel gases. Secondly, it absorbs the energy released in the fusion reaction, from whence it is removed as heat for electrical power generation. In addition, the blanket will contain breeder material from which further supplies of tritium fuel are produced by nuclear transmutation. The first wall in particular will be subjected to intense particle and radiant energy fluxes, elevated temperatures and cyclic thermal and mechanical stresses.

The service lifetime and reliability of the first wall or blanket is considered to be one of the principal factors governing the commercial development of fusion energy. The economic penalty incurred through the loss of system availability during replacement operations on first wall or blanket components demands the employment of structural materials offering a certain specified service life under severe operating conditions. Several categories of metallic alloys are currently under consideration as candidate materials[1]. These include austenitic stainless steels, precipitation-hardened Fe-Ni-Cr alloys, alloys based on titanium and refractory alloys. The results of recent fission neutron irradiation experiments indicate that a further group of alloys, namely ferritic/martensitic stainless steels, may offer the possibility of longer lifetimes on account of their resistance to radiation damage.

The ferromagnetism exhibited by martensitic stainless steels has hitherto been regarded as a possible barrier to their use in magnetic confinement fusion devices and the main purpose of this paper is to assess the probable impact of their magnetic properties on reactor operation. The first part of the paper provides a general introduction to the different groups of stainless steels and includes a brief description of particular properties of martensitic steels relevant to their potential use in fusion reactors. The second part, based largely on the results of recent work by the research group at the General Atomic Company, discusses the implications of ferromagnetism in martensitic stainless steels in relation to their utilisation as first wall or blanket materials.

2. THE STRUCTURE AND CONSTITUTION OF STAINLESS STEELS

Stainless steels are generally defined as ferrous alloys containing a minimum of about 12% chromium in solid solution for corrosion resistance [2-4]. Within this definition there exist four main categories of stainless steels, namely the ferritic, austenitic, martensitic and precipitation-hardenable groups, based on compositional, microstructural and crystallographic differences. Austenitic stainless steels generally contain more than 12% Cr whereas ferritic or martensitic steels for application in chemically non-aggressive environments can have less than 12% Cr, e.g. 9% Cr-Mo steel. The fundamental characteristics of these classes can be understood with reference to the iron-chromium equilibrium phase diagram[2] shown in Fig 1.

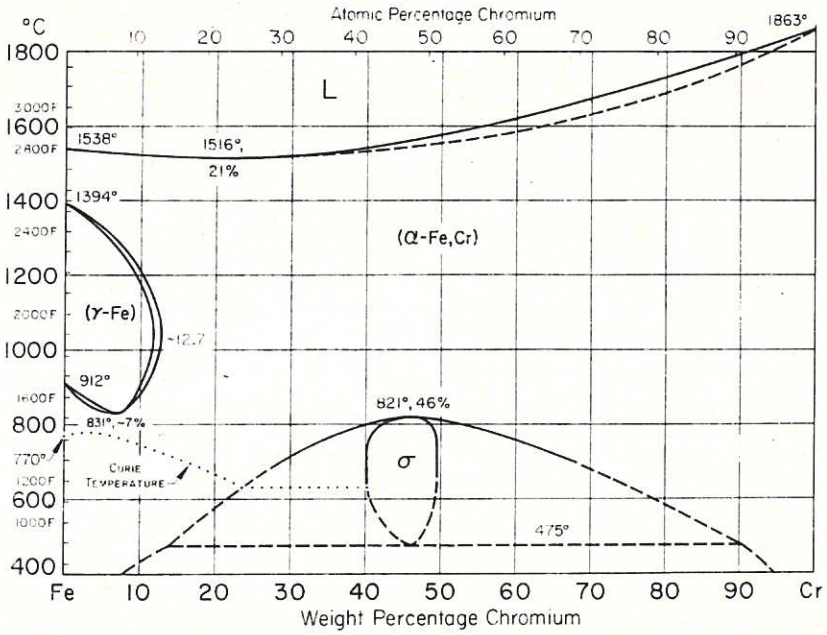

Fig.1 The iron-chromium phase diagram (from 'Metals Handbook', vol.8, 8th ed., American Society for Metals).

The most basic of the alloy phases are derived from the allotropic forms of pure iron. Below 910°C iron has a body centred cubic (bcc) structure known as α ferrite. From about 1400°C to the melting point at 1538°C the structure is again body centred cubic and this allotrope is known as δ ferrite. The α and δ ferrites have the same crystal lattice and are physically indistinguishable. Between 910°C and 1400°C the stable phase is γ ferrite, also known as austenite, with a face centred cubic (fcc) structure. These phase relationships can be summarised thus:

$$\alpha \xrightarrow[910^{o}]{} \gamma \xrightarrow[1400^{o}]{} \delta \xrightarrow[1538^{o}]{} \text{liquid}$$

The ferromagnetism of iron occurs only within the α phase, though it is a property only indirectly related to the crystalline structure and disappears at the Curie point of 770°C without any appreciable change in structure. In some older literature iron above the Curie point but below 910°C is referred to as β ferrite. There is little justification for this distinction, however, since α and β iron have identical crystal lattices, and it is now more common to include both α and β forms under the name of α ferrite.

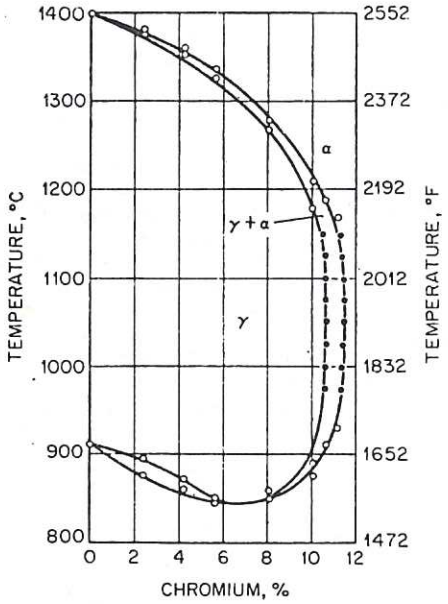

Fig.2 The γ loop of the Fe–Cr phase diagram for nearly pure alloy with additions of 0.004% C and 0.002% N by weight (from Ref.5).

The γ phase region in the iron-rich portion of the binary Fe-Cr equilibrium diagram is shown in greater detail in Fig 2. Referring to the lower part of the boundary it is evident that the addition of chromium up to about 7% reduces the temperature of the α to γ transition point. Above 7% Cr the temperature range over which austenite exists decreases until, above about 12% Cr, no transformation occurs and α ferrite exists at all temperatures. On account of this action, chromium is sometimes referred to as a ferrite-forming element, a property shared by other elements such as molybdenum, silicon and aluminium. The presence of certain other elements, notably nickel, manganese, carbon and nitrogen, causes a broadening of the austenite field and these are known as austenite-forming elements. The effect of varying nickel and chromium equivalents on the constitution of stainless steels is often predicted by means of the Schaeffler diagram, given in Fig 3. It should be noted that this diagram describes the phase constitution at ambient temperature following rapid cooling from elevated temperatures. The Fe-Ni and Fe-Ni-Cr equilibrium diagrams [2] should be consulted for the structures and constitutions at high temperatures.

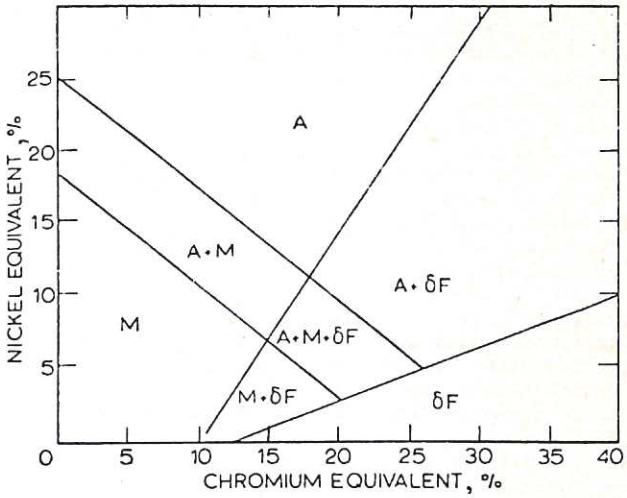

A = austenite; M = martensite; δF = delta ferrite

Fig.3 Schaeffler diagram indicating the effect of nickel and chromium equivalents on the constitution of stainless steels (from Ref.6).

2.1 Ferritic stainless steels

The ferritic stainless steels, containing 15-30% Cr and essentially no nickel, are in principle structurally simple. At normal temperature they consist of a Fe-Cr solid solution having a bcc α-ferrite structure and they remain essentially ferritic up to the melting point. The upper chromium limit is arbitrary and is intended to include all commercial Fe-Cr alloys. Carbon is practically insoluble in the α matrix and most of the element present occurs in the form of finely-dispersed carbides. Thus binary Fe-Cr alloys free from carbon are essentially stainless irons. Some typical compositions are given in Table 1.

TABLE 1 Some typical ferritic stainless steel compositions
These alloys are body-centred cubic, ferromagnetic and not heat treatable.

AISI type no*	nominal composition, % by weight C	Mn	Cr	others
430	0.08 max	1.0	16-18	
430F	0.12 max	1.25	16-18	0.6 Mo max
446	0.2 max	1.5	23-27	0.25 N max

*The AISI classification system for stainless steels is described in Appendix A.

As is evident from the binary phase diagram (Fig. 1), alloys containing more than about 12% chromium do not undergo any phase change up to the melting point and cannot therefore be significantly strengthened by heating them to high temperature and then rapidly cooling. In practice, a limited degree of strengthening and hardening can occur on heating a ferritic alloy above 850°C. This effect is mainly due to grain growth and the presence of small volumes of austenite which revert to martensite, a form of α-iron, on cooling. Exploitation of these processes for strengthening is generally undesirable, however, because the alloys become embrittled and their ductility and toughness at normal temperature are severely reduced. Precipitation of the chromium-rich ferrite phase can occur in the ferritic stainless steels with chromium contents in excess of about 14% at temperatures in the range 300-500°C, giving rise to the well-known "475°C embrittlement" phenomenon [7]. At higher temperatures δ-phase precipitation can also occur, again leading to embrittlement[7].

The ferritic grades can be cold-worked and annealed. They are generally more corrosion resistant than the martensitic grades but less so than the austenitic alloys. In general, the ferritic steels have strengths comparable with or even higher than those of the austenitics at lower temperatures though the ferritic steels rapidly lose their strength and become appreciably more ductile than the austenitics at temperatures above 500° - 600°C. The ferritic steels exhibit the ductile-brittle transition temperature phenomenon characteristic of body centred cubic structures. The metallurgical characteristics of the ferritic steels, particularly the grain size and cleanliness, are important in determining the ductile-brittle transition temperature, resistance to fast fracture, and high-temperature tensile and creep-rupture properties.

2.2 Martensitic stainless steels

Martensite is a metastable phase formed from austenite when the material is cooled sufficiently rapidly to suppress the formation of pearlite (a eutectoid mixture of ferrite and cementite, Fe_3C) and other diffusion-controlled reactions and consists of a supersaturated solid solution of carbon in α iron. Though it has the same composition as austenite the unit cell is deformed by the high carbon content and is tetragonal instead of body centred cubic. Martensite produced by quenching simple iron-carbon solid solutions is stable only below about 150°C and is rapidly formed from quenched austenite at this temperature and below. The temperature at which martensite begins to form during the quenching of austenite is known as the 'martensitic start temperature' M_s and decreases in the following way with increasing carbon content:

%C	0.02	0.2	0.4	0.8	1.2
M_s(°C)	520	490	420	250	150

M_s is also dependent on the alloy content and the following empirical formula can be used to estimate M_s from the chemical composition, provided all carbides are initially dissolved in the austenite:

$$M_s(°C) = 561 - 474(\%C) - 33(\%Mn) - 17(\%Ni) - 17(\%Cr) - 21(\%Mo)$$

The M_s temperature for the 12% Cr steels is thus about 300°C.

The martensitic alloys were developed to satisfy a need for stainless steels that could be strengthened and hardened by heat treatment. This aim is achieved through the addition of carbon to the binary Fe-Cr system, thus producing an alloy that responds to a quench temperature cycle. The compositions of some typical martensitic alloys are given in Table 2.

There are two essential requirements for the formation of a martensitic stainless steel. Firstly, there must be an austenite field in the equilibrium diagram and, secondly, at least 12% chromium must be present in solution in the structure in order to develop high passivity. Reference to Fig. 2, which shows the γ region of the binary Fe-Cr system, indicates that the addition of one or more austenitising elements is necessary to extend the austenite field to chromium levels sufficiently high to give good corrosion resistance. Figure 2 also reveals the existence of a narrow transitional region between the γ loop and the α field, representing the coexistence of both α and γ phases.

The presence of austenitising elements, carbon and nitrogen in particular, can greatly extend the γ loop toward higher Cr levels. The influence of carbon, nitrogen and nickel in this respect is illustrated by Figs. 4 and 5. The extent of the two-phase (α + γ) field has been omitted from these diagrams.

Additions of carbon and nitrogen are seen to cause a substantial expansion of the outer boundary of the α + γ two-phase region to higher Cr levels, together with a shift of the extremity of this region toward higher temperatures. At 0.2% carbon, for example, the loop is expanded to 26% Cr and the point of greatest expansion is raised to about 1300°C, as compared with 1075°C for a pure Fe-Cr alloy. Nitrogen acts in a similar way; 0.25% N for example moves the point of maximum width of the mixed phase from 11.5% Cr for the pure alloy, to 28% Cr and the corresponding temperature from 1075 to 1250°C. Carbon and nitrogen are incorporated into the structure as interstitials, whereas heavier elements such as nickel and manganese enter by substitution. It is perhaps worth mentioning that, while the proportion of carbon or nitrogen present in the structure may seem very small, the content expressed in terms of the atomic concentration is about 5 times larger than that measured on the percentage weight basis thus, for example, 0.2% C by weight corresponds to an atomic concentration of about 1%.

The possibility of utilising the martensite - austenite phase change depends very much on the

TABLE 2 Some typical martensitic stainless steel compositions
These alloys are body-centred cubic, ferromagnetic and heat treatable

AISI type no	nominal composition, % by weight C	Mn	Cr	Ni
403	0.15 max	1.0	11.5-13	
410	0.15 max	1.0	11.5-13	
420	0.15 max	1.0	12-14	1.2-2.5
431	0.2 max	1.0	15-17	

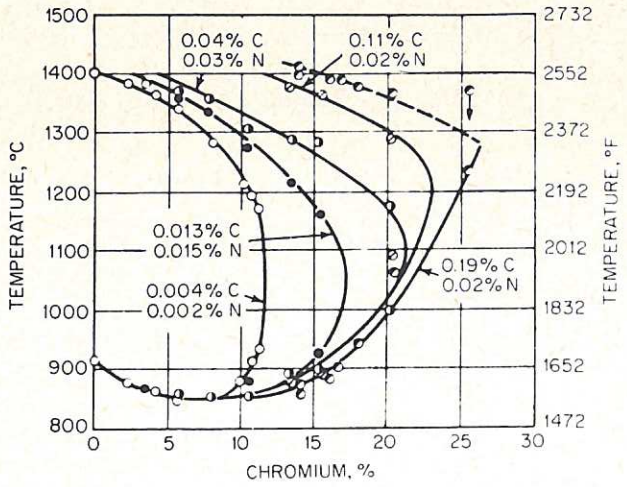

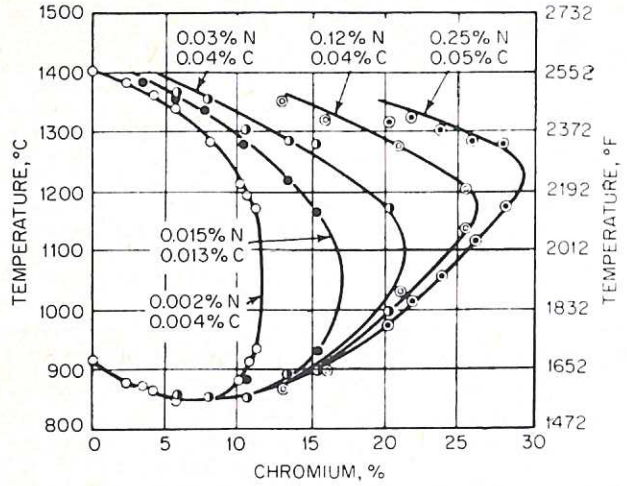

Fig.4 Diagram showing shifting of the $(\gamma + \alpha)/\alpha$ phase boundary in the Fe–Cr system through increasing additions of carbon or nitrogen (from Ref.5).

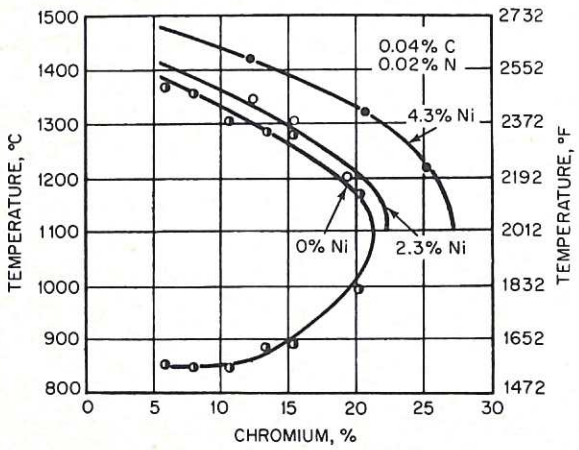

Fig.5 Diagram showing shifting of the $(\gamma + \alpha)/\alpha$ phase boundary in the Fe–Cr system through increasing additions of nickel (from Ref.5).

chromium content and on the level of austenitising elements. At low Cr content a relatively low interstitial level suffices to give a two-phase structure when heated to around 1100°C. With higher proportions of Cr the two-phase structure can only be attained at high interstitial levels. In general, a Cr content exceeding about 13% no longer allows an extensive $\alpha \rightarrow \gamma$ transformation on heating, hence grain refinement and hardening by heat treatment and quenching are not possible.

In addition to its effect in extending the $(\alpha + \gamma)$ field, carbon leads to the formation of the complex carbides $(Cr,Fe)_7C_3$ and $(Cr,Fe)_{23}C_6$, which precipitate mainly at the grain boundaries and on lath boundaries during tempering. Quenching a 12% Cr steel containing 0.1%C from a temperature of about 1100°C will result in the formation of martensite. The carbon is retained in solution and distorts the bcc α-ferrite cell to a body centred tetragonal martensite cell. During subsequent tempering, however, the excess carbon and nitrogen are precipitated as a series of complex carbides and nitrides which can profoundly influence the properties of the alloy. The martensite will eventually revert to α-ferrite when the excess interstitials have thus been removed. The tempering process, carried out at temperatures in the region of 650°C, removes the hardness and brittleness characteristic of martensite and produces a softer but tougher material.

The corrosion resistance of the martensitic group is generally lower than that of the ferritic and austenitic groups and the choice between martensitic or ferritic alloys is usually based on the importance of corrosion resistance relative to the strength, hardness and wear resistance required. The properties of the 12% Cr martensitic steels depend sensitively on the composition and structure and references 8 and 9 should be consulted for details of the structure-property relationships.

2.3 Austenitic stainless steels

The austenitic stainless alloys are formed by the addition of a face centred cubic element such as nickel or manganese to the Fe-Cr binary system. As mentioned above, the addition of austenitising elements such as nickel can result in a considerable expansion of the γ phase and may tend to suppress the formation of α ferrite. An austenite structure stable at room temperature can be formed with a minimum of 8% Ni present and the austenitic stainless steels can be defined as those Fe-Cr alloys containing sufficient alloy additions of nickel or manganese and nitrogen to yield an austenitic structure stable at room temperature.

A carbon-free alloy containing 18% Cr would need about 12% Ni to form a fully austenitic structure at the solution-treatment temperature of about 1050°C. Carbon is a strong austenite former, however, and an 18Cr-8Ni-0.1C alloy is fully austenitic above 900°C, though the temperature, M_s, at which martensite starts to form is only just below room temperature and the austenite can partially transform to martensite during cold working or under refrigeration. In order to avoid this effect the M_s temperature can be depressed through the addition of further alloying elements so that a stable austenitic structure is retained after cooling from the solution-treatment temperature to room temperature.

The austenitic stainless steels represent the largest group of stainless alloys in commercial use, accounting for about 70% of the total. The commonest ones are Fe-Cr-Ni alloys of the AISI 300 series which occupy a dominant position by virtue of their high corrosion resistance, easy fabricability

and the varied combinations of specific properties given by different compositions within the group. Some typical compositions are indicated in Table 3. Since these alloys do not undergo any phase transformation during heating they cannot be hardened by heat treatment. They can, however, be significantly strengthened and hardened by cold working. The carbon content is held to a minimum or, in the case of some grades such as 321 and 347, is stabilised by the addition of niobium or titanium to avoid intergranular corrosion and loss of toughness caused by carbide precipitation in the grain boundaries following exposure to elevated temperature.

The structure-property relationships for austenitic stainless steels forms a subject too wide to allow adequate treatment here, since the emphasis in this paper is on ferritic/martensitic steels. The reader is referred to the literature [10] for a discussion of this subject.

2.4 Precipitation-hardenable stainless steels

The fourth group of alloys comprises the general class known as precipitation-hardenable stainless steels, in which the technique of age-hardening or precipitation-hardening employed in other alloy systems is applied to the iron-based corrosion-resistant alloys.

The precipitation-hardenable group represents a wide variety of alloy types with a diversity of often quite complex hardening mechanisms. A detailed discussion of this group of alloys would be out of place here and the interested reader is referred to the bibliography for further details.

2.5 Magnetic properties

In Fig.1 the dotted line represents a third transformation point in the Fe-Cr system, namely the Curie point, above which iron is paramagnetic and below which it is ferromagnetic. A review of the basic terms and concepts employed in magnetism is given in Appendix B. Paramagnetic iron has a relative permeability practically equal to unity and is commonly described as non-magnetic, whilst ferromagnetic iron has a relative permeability much greater than unity, the exact value depending on composition, temperature, the magnitude of the applied field and on the history of the specimen. If the fcc γ structure is maintained at lower temperatures then the alloy will remain paramagnetic or 'nonmagnetic'. Thus austenite is nonmagnetic at room temperature whilst α ferrite, with bcc structure, is ferromagnetic. Some of the possible implications of employing ferromagnetic stainless alloys for the first wall or blanket in a magnetic confinement nuclear fusion reactor are examined in the following sections.

3. MARTENSITIC STAINLESS STEELS AS STRUCTURAL MATERIALS IN FUSION REACTORS

The first wall of a fusion reactor will be exposed to neutrons, neutral atoms and ions of He, D and T, and X radiation from the plasma. Of the energy released in the fusion reaction D + T → He + n, 14.1 MeV is carried by the neutron and 3.5 MeV by the alpha particle. An additional energy of about 2.4 MeV per fusion neutron is gained from transmutations in the breeding material, giving a total energy release of approximately 20 MeV per fusion event. The power level of a reactor is commonly expressed in terms of the rated wall loading P_w, defined as follows:

$$P_w = \frac{(W_n + W_\alpha + W_c)N}{A}$$

where W_n = neutron energy, 14.1 MeV
W_α = alpha particle energy, 3.5 MeV
W_c = net energy gain in blanket ≈ 2.4 MeV
N = number of D-T fusion events per second
A = area of first wall

Thus P_w represents the total power density at the first wall. An alternative parameter employed by some authors is the neutron wall loading P_n, which is related to P_w through the equation

$$P_n = \frac{W_n N}{A} \approx 0.7\, P_w$$

Roughly 10% of the energy of the incident neutrons is deposited in the first wall, the remainder being absorbed by the blanket. In the absence of a divertor the energy associated with the neutral atoms, ions and photons is almost completely intercepted by the first wall.

The target wall loading for an economic fusion reactor is about 10 MWm^{-2}, corresponding to a neutron flux of 3×10^{19} $m^{-2}s^{-1}$. Assuming a duty cycle in which first wall/blanket components are utilised for 2 years at a load factor of 0.75 and are then replaced, the corresponding exposure equivalent would be in the region of 15 $MWyrm^{-2}$.

For acceptable thermal efficiency the blanket will need to operate at a temperature in the region 400-500°C and may be subject to substantial temperature excursions over the operating cycle. Severe fatigue problems can be expected as a result of both thermal and mechanical cycling, particularly in reactors operating in a pulsed mode. For example, the duty cycle for reactors having a pulsed burn phase of duration 1000s would involve about 5×10^4 stress cycles, whilst that of continuous burn reactors, such as STARFIRE, would entail about 500 stress cycles. The integrity of the first wall as a vacuum boundary must be strictly maintained since any leakage of coolant or breeder material into the plasma chamber would lead to quenching of the fusion reaction. Moreover, after a period of operation, the first wall and blanket structure will be highly radioactive. Replacement of these components will therefore involve remote handling operations with the reactor shut down and will entail a substantial reduction of plant availability. The service life of such structures will thus exert a strong influence on the economics of fusion power generation.

The lifetime of first wall/blanket structures will most probably be limited by the effects of

TABLE 3 Some typical austenitic stainless steel compositions
These alloys are face-centred cubic, paramagnetic and not heat treatable

AISI type no	nominal composition, % by weight				
	C	Mn	Cr	Ni	others
201	0.15 max	7.5	16-18	3.5-5.5	0.25 N max
301	0.15 max	2.0	16-18	6-8	
304	0.08 max	2.0	18-20	8-12	
316	0.08 max	2.0	16-18	10-14	2-3 Mo
347	0.08 max	2.0	17-19	9-13	(10 x %C) Nb-Ti min

radiation damage caused by the high energy neutrons. The exposed materials will be subject to irradiation swelling and creep, embrittlement and loss of ductility and surface effects such as sputtering and blistering. The radiation-induced damage will be exacerbated by thermal and mechanical cycling. The integrated neutron flux (termed the fluence) does not provide an accurate indication of the radiation damage because the latter is sensitive to the energy spectrum of the neutrons. The mean number of displacements suffered by a lattice atom during a period of irradiation gives a more useful measure of the integrated effect of the neutron flux since this parameter is less dependent on neutron energy. This quantity is known as the number of displacements per atom or dpa. About 150 dpa would be expected for a stainless steel exposed to a fusion neutron fluence corresponding to $15 MWyrm^{-2}$.

The neutrons can also cause nuclear transmutations in the structural materials. The nickel component in austenitic stainless steels, for example, undergoes (n,γ) and (n,α) reactions with thermalised neutrons:

$$Ni^{58} + n \rightarrow Ni^{59} + \gamma$$
$$Ni^{59} + n \rightarrow Fe^{56} + \alpha$$

The helium and hydrogen formed in (n,α) and (n,p) reactions may accumulate in bubbles on the grain boundaries at high temperatures and strongly degrade the mechanical properties of the irradiated material.

Since neutron sources providing an energy spectrum and flux density pertinent to a fusion reactor are so far unavailable, the effects of irradiation in the fusion environment can be assessed only indirectly through simulation experiments. Most tests to date have been performed with the aid of fission reactors though some have utilised ion beams from particle accelerators. Such simulations suffer from the important limitation that they do not adequately represent the much higher rates of generation of hydrogen and helium expected with fusion neutrons. Thus irradiation in a fission reactor may typically produce a helium concentration of order 10 appm, as compared with 1000 appm anticipated in a fusion reactor. Tests under conditions more closely resembling the fusion reactor environment will evidently be needed to indicate the life expectancy of reactor components.

Several classes of candidate materials are currently being considered for first wall structures[1,11]. These include austenitic stainless steels[12], martensitic stainless steels[13-15], precipitation-hardened Fe-Cr-Ni alloys, refractory alloys based on titanium and refractory alloys based on vanadium and niobium. The results of fission reactor irradiation tests suggest that the Fe-Cr martensitic stainless steels might offer a significantly longer lifetime than some of the alternative candidate materials and a number of studies devoted to the assessment of this class of material have recently been published[13-15]. Of the candidate materials mentioned above, only the martensitic stainless steels show ferromagnetic behaviour and it will be necessary to assess the implications of incorporating ferromagnetic structural materials in fusion reactors employing magnetic confinement.

The martensitic alloys under consideration fall within the general group of ferritic steels containing roughly 9 to 13% Cr, together with small proportions of various strengthening elements such as molybdenum. Such steels, generally in the normalised and tempered condition, are already widely used in high temperature applications, where they can compete favourably with austenitic alloys at temperatures up to 600°C. The commercial Sandvik alloy HT-9 with composition 12Cr-1Mo-0.3V may be regarded as typical of this class. This and similar alloys have been utilised for several years in such applications as steam and gas turbines, jet engines, steam pipes and boiler tubes [16] and are currently being considered for future use in thermal and fast reactors. For the purpose of their evaluation studies [13-15] the General Atomic research group selected the alloy HT-9 as representing a typical martensitic alloy. It is in fact the only commercial alloy among the group of six prime candidate materials identified by the National FBR Cladding/Duct Materials development programme. While newer alloys such as 9Cr-1Mo currently under development may eventually prove superior, HT-9 has the considerable advantage of possessing a relatively broad and expanding data base and a history of commercial applications in arduous environments.

4. SOME RELEVANT PROPERTIES OF MARTENSITIC STAINLESS STEELS

4.1 Composition

The nominal composition of the representative martensitic alloy HT-9 is given in Table 4. The composition of the austenitic alloy type 316 is also included for comparison.

For extended high temperature service the alloy is usually heat treated at 1050°C for half an hour, air cooled, then tempered at 780°C. Tempering at this relatively high temperature does not develop maximum strength but ensures high stability of the tempered martensite and of the strengthening carbide precipitates for service temperatures up to about 600°C.

4.2 Mechanical Strength

The temperature variation of minimum ultimate tensile strength is shown in Fig.6, taken from Ref.15, for HT-9 and a number of other candidate first wall materials including type 316 annealed stainless steel and 20% cold-worked 316 stainless steel. The short term strength of HT-9 evidently decreases rapidly above 500°C. It is roughly comparable with that of the austenitic stainless steel type 316 at temperatures up to 600°C. The long term strengths of HT-9 and 316 are compared in Table 5, which shows the maximum allowable stress intensities as defined by the ASME Boiler and Pressure Vessel Code for elevated temperature design of class 1 nuclear components.

In a fusion reactor with pulsed operation, thermal stresses are liable to cause cyclic and creep fatigue damage. The resistance to thermal

Table 4 - Nominal composition of representative alloy HT-9 and alloy 316

alloy	Fe	Cr	Ni	Mo	W	V	Si	Mn	C
HT-9	85.25	11.5	0.5	1.0	0.5	0.3	0.25	0.5	0.20 weight
316	66.5	17	12	2.5				2.0	0.08 %

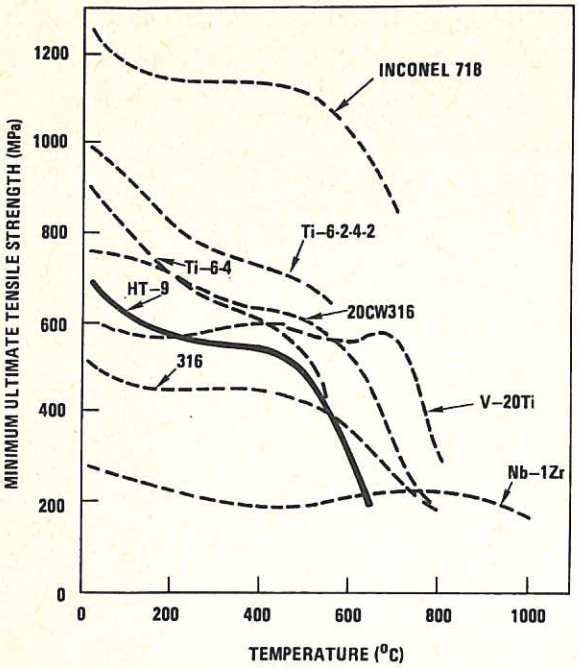

Fig.6 Graph showing the minimum ultimate tensile strength of HT-9 and other candidate alloys as a function of temperature (from Ref.15).

stress is usually represented by a parameter M, defined by

$$M = \frac{2\sigma K(1 - \nu)}{\alpha E} \qquad (watt.m^{-1})$$

where σ = yield strength
K = thermal conductivity
ν = Poisson's ratio
α = thermal expansion coefficient
E = Young's modulus

The resistance to thermal stress increases with increasing M. The thermal stress resistance of HT-9 at 500°C is compared with that of alternative materials in Table 6. The considerably higher resistance of HT-9 in comparison with alloy 316, for example, is largely attributable to the higher thermal conductivity and lower thermal expansion coefficient of HT-9. The Ti alloys and the precipitation-strengthened Ni alloy Inconel 718 have slightly higher thermal stress resistances than HT-9.

Table 6
Thermal stress resistance of some candidate alloys at 500°C

Material	Thermal stress resistance M (kWm)
316 annealed	1.3
20% CW 316	4.9
HT-9	8.5
Ti-6Al-4V	10.2
Ti-6Al-2Sn-4Zr-2Mo	10.4
Inconel 718	10.7
V-20Ti	12.3
Nb-1Zr	19.8

.4.3 Radiation damage

One of the principal advantages of the martensitic stainless steels is their relatively high resistance to neutron radiation damage. Information on creep, void swelling and embrittlement in HT-9 has been gained during the course of the fast breeder reactor programme in the U.S.A. but has not yet been generally released. The following description of radiation effects is based on a qualitative assessment by Rawls et al [15] partly based on data from EBR-II. According to these authors, HT-9 has a higher in-reactor creep resistance than the 20% cold-worked type 316 stainless steel (20% CW 316) to temperatures in excess of 600°C. Void swelling in HT-9 appears to be at least a factor of 10 less than that in 20% CW 316 and current data indicate swelling even lower than the 3.7%, 500°C peak swelling at 150 dpa reported previously for HT-9 under irradiation conditions simulated by heavy ion bombardment (17). A peak swelling of about 35% at 580°C and 150 dpa is predicted for 20% CW 316 steel [18].

The resistance of ferritic and martensitic alloys to radiation-induced void swelling has also been demonstrated by recent fast reactor irradiation experiments in Britain and France [19-25]. In particular, Little and coworkers have described observations on several commercial alloys including a 2.25Cr-1Mo low alloy steel, Fe-14Cr-4Al alloy and three 12% martensitic steels designated FI, FV448 and CRM-12. These observations support the proposition that ferritic/martensitic alloys as a general class have favourable void swelling characteristics, and resistance to high temperature irradiation (helium) embrittlement together with good mechanical properties and low neutron absorption cross-sections relative to austenitic stainless steels and alternative nickel-based alloys.

Whilst the evaluations to date involve only low helium levels and low helium/dpa ratios relative to fusion neutron conditions, the retention of tensile ductility by HT-9 appears to be superior to that of 20% CW 316 (especially when tested above the irradiation temperature) and much greater than that of the precipitation-strengthened nickel alloys up to 600°C. Moreover, the microstructure of HT-9 appears to be stable under irradiation in the pertinent temperature range. Ferritic and martensitic steels exhibit the ductile-brittle transition phenomenon typical of body centred cubic metals. Such metals transform over a narrow temperature range from a state in which failure under tensile stress occurs by brittle fracture, to a condition of greater softness, in which the

Table 5

Allowable 300,000 hour design stresses, S_{mt}, based on the criteria of ASME Boiler and Pressure Vessel Code Case N47. From Ref. 15.

Alloy	Maximum allowable stress intensities, S_{mt} (MPa)					
	20°C	400°C	500°C	550°C	600°C	650°C
HT-9	227	196	110	62	32	14
316	138	110	108	87	50	31

material deforms plastically and failure occurs by ductile fracture. The temperature at which this change occurs is termed the ductile-brittle transition temperature or DBTT. Irradiation has the effect of raising the DBTT, the shift being closely related to the degree of irradiation hardening. The effect of fast reactor irradiation on the impact resistance and fracture toughness of HT-9 alloy has been investigated by Smidt, Hawthorne and Provenzano[26]. In these studies the alloy was irradiated in EBR-II at 419°C to a fluence of 1.1 x 10^{26} nm^{-2} (E > 0.1MeV), corresponding to a damage level of about 6 dpa. This irradiation was found to elevate the DBTT from the initial value of 5°C to 113°C and to increase the room temperature yield strength from 653 MPa to 971 MPa. After irradiation the fracture toughness was measured as 170 $MPam^{\frac{1}{2}}$ well above the DBTT and 45 $MPam^{\frac{1}{2}}$ below it. Irradiation decreased the upper shelf energy (Charpy V notch test) from 170J to 88J, observed at 150°C, though the measured value increased with test temperature to 115J at 427°C. Temper embrittlement at 538°C after 5000h aging was also reported.

In general the radiation embrittlement tends to saturate with increasing neutron dose and it is possible that the operating temperature of the first wall and blanket would always be above the DBTT of the ferritic/martensitic alloy. Care might be needed, however, to avoid brittle failure if the temperature fell below the DBTT, for example during reactor shutdown.

4.4 Induced radioactivity

A graphical comparison of the radioactivity associated with type 316 steel and with alternative materials is given in Fig 7. On the scale of this graph the curve for alloy HT-9 lies very close to that for the 316 steel. The activities plotted in this graph are taken from Ref. 28 and are based on an exposure to $1MWm^{-2}$ wall loading for 1 year[29].

The effects of induced activity in ferritic/martensitic steel blanket materials have also been considered by Rawls et al [15]. These authors adopted a blanket model consisting of a first wall, a Li_2O breeding zone and a graphite reflector. The breeding zone of thickness 0.25m, comprised 10% mechanical structure, the remaining volume being occupied by Li_2O with a packing density of 80%. Calculations of the induced activity were based on continuous operation for 6 years with a neutron wall loading of 1 MWm^{-2} [27]. The results are given in Table 7 for both 316 and HT-9 steels.

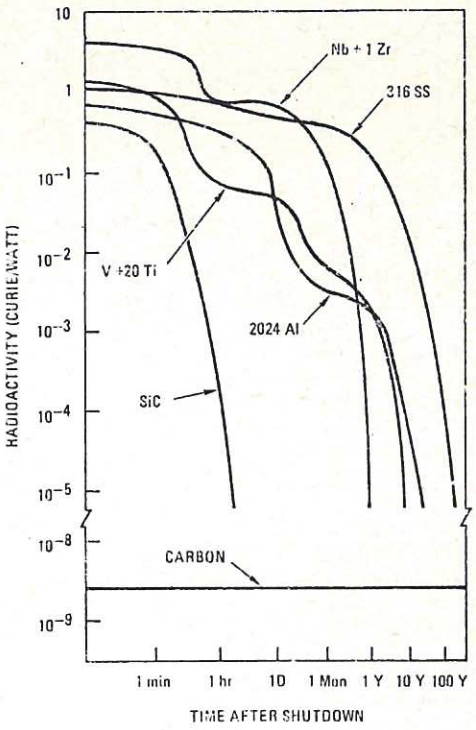

Fig.7 Curves showing decay of radioactivity following shutdown for several candidate first wall and blanket materials (from Ref.28).

It is evident that at shutdown the radioactivity in the HT-9 alloy is about 10% lower than that in the 316 alloy, whilst after 100 years it is less than half that in 316.

Table 8, from Ref 15, gives the calculated afterheat following shutdown. Initially, the afterheat is about the same for both materials but subsequently the HT-9 shows an appreciably lower level. Thus HT-9 shows marginally less pronounced post-irradiation activity than the austenitic alloy 316.

4.5 Weldability

The stainless steels in general demand care during welding to ensure good service performance of

Table 7
Radioactivity in 316 and HT-9 based blankets following 6 years of operation at 1 MWm^{-2} neutron wall loading

Time after shutdown	316 steel	HT-9 steel
	curies per watt (thermal)	
10 sec	1.31	1.17
1 day	7.8×10^{-1}	6.6×10^{-1}
1 month	6.6×10^{-1}	5.9×10^{-1}
1 year	3.7×10^{-1}	4.0×10^{-1}
100 years	4.3×10^{-5}	1.8×10^{-5}

Table 8

Post-operation afterheat in 316 and HT-9 based blankets following 6 years of operation at 1MWm^{-2} neutron wall loading.

Time after shutdown	units:	316 steel % of operating power	HT-9 steel
10 sec		1.4	1.3
1 day		1.5×10^{-1}	5.9×10^{-2}
1 month		1.3×10^{-1}	5.4×10^{-2}
1 year		4.7×10^{-2}	3.0×10^{-2}

the resulting weld. Ferritic steels are susceptible to excessive grain growth and development of brittleness; martensitic grades may suffer excessive hardening, with the attendant risk of cracking, whilst the austenitic grades have high thermal expansion coefficients and are subject to carbide precipitation. As a group, the austenitic grades are the most easily welded. With the martensitic steels care is needed to avoid too much martensitic hardening during air cooling following the welding operation. The resulting risk of cracking increases with the carbon content, the hardness and the degree of restraint. The potentially deleterious effects of welding can, however, largely be overcome through careful control of the welding conditions and through the application of appropriate pre-weld and post-weld heat treatments. Very few weld failures have been experienced in fossil-fuelled power stations employing 9% and 12% Cr steels [16] and it appears unlikely that the problems associated with the welding of these alloys would prove a major obstacle to their use.

4.6 Cost and availability

Comparative cost relations for various types and forms of stainless steels are given in Ref.2, though the actual prices quoted are somewhat out of date. These show a variation, by roughly a factor two, between the cheapest and most expensive commercially-available grades. Also, the prices of particular grades vary by about 30% depending on the basic finished form and the batch size. Current prices of some of the more common stainless steels are indicated in Table 9.

Owing to the high cost of nickel, the nickel-free ferritic and martensitic grades tend to be cheaper than the austenitic alloys with substantial nickel contents. This advantage may be reduced by the added cost of heat treatment required during the fabrication of components from martensitic alloys and, in the case of steels containing molybdenum, by the present high cost of this element. The alloy HT-9 is at present available only in a limited variety of forms but the cost of the basic material appears to be comparable to that of type 316 stainless steel.

In the case of intricate fabrications, such as those likely to be required in fusion applications, the cost of the basic material is likely to represent only a fraction of the cost of the finished item. For structural components close to the plasma the basic material cost is unlikely to be a major factor in any choice between alternative grades of stainless steel. It could, however, exert a decisive influence on the choice of material for peripheral structures, which require large quantities of material but with less demanding fabrication and special property requirements.

Chromium, a basic constituent of stainless steels, is not a particularly abundant element and it is possible that a global scarcity of this element, perhaps accelerated by a high demand for structural stainless alloy by the nuclear industry around the year 2000, may impose an additional constraint on the choice of reactor blanket/first wall materials. Were such a constraint to apply it would favour the use of chromium-lean alloys such as the martensitic grades or specially developed low-chromium grades.

5. THE MAGNETIC PROPERTIES OF MARTENSITIC STAINLESS STEELS

There appears to be little detailed information on the magnetic properties of ferromagnetic stainless steels, particularly in relation to their dependence on factors such as temperature and metallurgical and mechanical history. Measurements

Table 9 - Current 1980 prices of various stainless steels, in the form of cold-rolled 5 mm sheet, and of the major alloying elements. The costs are in £/tonne.

Austenitic grades type	cost	Ferritic grades type	cost	Martensitic grades* type	cost	Alloying elements	
304	1075	409	1000	403	1000	Cr	450
304L	1850	430	1000			Ni	4,000
321	1850	434	1300			Mo	12,000
316	2350	444	1600				
316L	2450						

* The martensitic grades do not readily allow price comparison since they are not normally produced in cold-rolled forms.

on the alloy HT-9 have been reported by the research group at the General Atomic Company [13-15], whilst measurements on a 9% Cr 2% Mo alloy have been performed by the above mentioned group and also by Praeg [30]. A brief review of ferromagnetism, including definitions of some of the pertinent terms, such as permeability, is given in Appendix B.

5.1 Measurements by the General Atomic Company research group

The alloy HT-9 is a hard magnetic material manifesting a large area within the hysteresis loop, the shape of which varies with the magnitude of the inducing magnetic field. The magnetic properties also depend on the mechanical history of the material and are affected by heat treatment and working. References 14 and 15 describe two sets of measurements on HT-9. In the first set, a hollow cylinder of the alloy, having a length many times the outer radius, was placed in a steady longitudinal magnetic field. Two sets of coils were wound around the cylinder and the ratio, r, of their measured mutual inductance to the value calculated for the same coil arrangement in vacuo was determined at 200°C. The results are given in Table 10.

It is seen that the ratio decreases from 23 at zero bias field and approaches unity for bias fields greater than about 800 kAm^{-1}. Because the sample only partly filled the solenoid and had an unspecified geometry, the above observations must be regarded as qualitative. They serve to show, however, that a bias field of about 800 kAm^{-1}, applied parallel to the excitation field, suffices to saturate the material and reduce its effective relative permeability to unity.

In the second experiment the alternating field permeability and the saturation flux density were measured on a ring sample as a function of the temperature and the bias field applied perpendicular to the plane of the ring. A toroidal sample of the alloy under investigation was wound with primary and flux measurement windings and placed in the field of a superconducting solenoid, which could provide a bias field up to about 4 MAm^{-1}, directed along the major axis of the toroid. The field produced by the current in the primary winding was thus orthogonal to the generally much stronger steady bias field. This arrangement forms the basis of a standard method of measuring both the saturation and low-field magnetic properties in the same sample and has been described by Graham [31] and by Zijlstra [32]. In this configuration the toroidal field causes the magnetisation vector to perform small oscillations about the static field vector and it may be shown that the low-field AC permeability thus measured approximates to $(B_o + B_s)/B_o$, where B_o is the flux density in the specimen due to the bias field alone and B_s is the intrinsic flux density corresponding to complete magnetic saturation.

As shown by the results in Table 11 the AC permeability of HT-9 alloy decreased from a value of 76 at zero bias field to a value of about 1.2 for bias fields in excess of 1.6 MAm^{-1}.

Further experiments were conducted by the General Atomic group to compare the magnetic behaviour of two representative martensitic stainless steels 9Cr-2Mo and 12Cr-1Mo (HT-9), under simulated tokamak reactor conditions and to measure the saturation flux density B_s as a function of temperature. The observations were made on toroidal samples in the way described above. In addition to providing the magnetising field, the primary winding served as a heater which could raise the temperature of the sample to about 500°C. The hysteresis loops were recorded oscillographically, using an alternating field of frequency 60 Hz and maximum amplitude 24 kAm^{-1}. Further experimental details are given in Ref. 15.

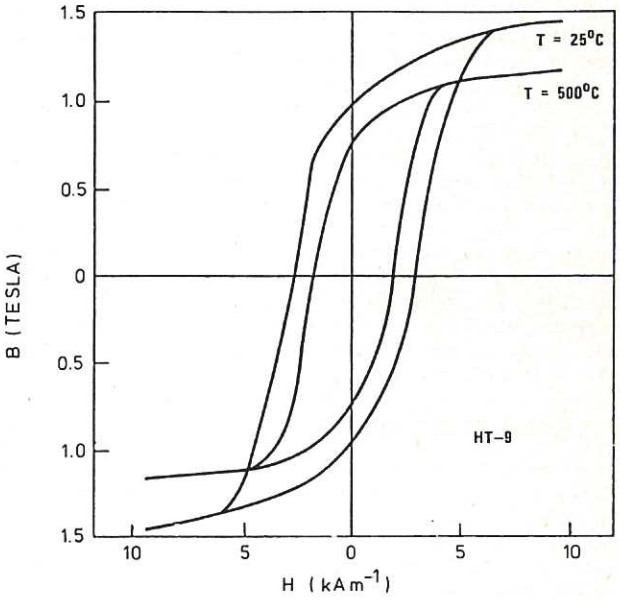

Fig.8 Comparison of the hysteresis loops for HT-9 alloy at room temperature and 500°C, according to Ref.15.

Table 10
Ratio r of measured mutual inductance of the coils to calculated mutual inductance without specimen as function of bias field at 200°C

Applied magnetic field (kAm^{-1})	0.0	48	80	240	800	2400
r	23	4.5	2.7	1.2	1.0	1.0

Table 11
AC permeability of HT-9 alloy at 315°C as a function of bias magnetic field

Bias magnetic field (MAm^{-1})	0.024	0.24	0.48	0.96	1.75
relative permeability	76	73	12	2.0	1.2

Figure 8 shows a comparison of the hysteresis loops for HT-9 steel at room temperature and a typical reactor operating temperature of 500°C. As would be expected, the area of the loop and the saturation flux density decrease with increasing temperature. The loops for the two materials 12Cr-1Mo and 9Cr-2Mo at 500°C are compared in Fig. 9, which shows the 9% Cr alloy to have a saturation flux density about 20% higher than that of the 12% Cr alloy. These results are summarised in Table 12.

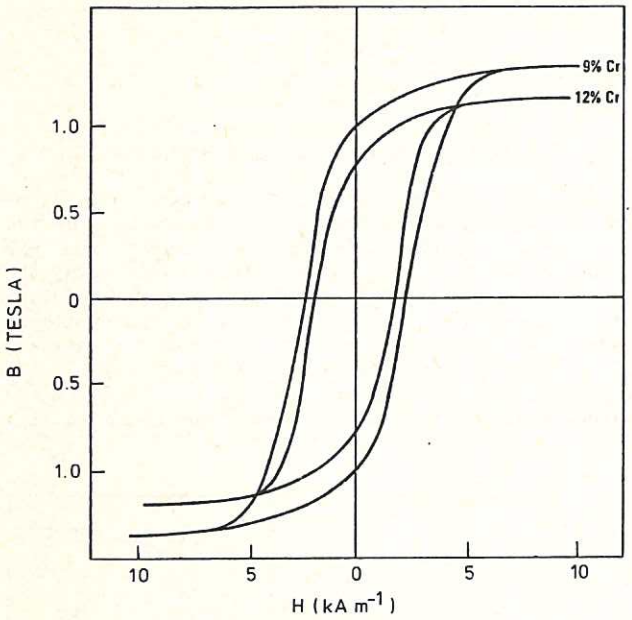

Fig.9 Comparison of the hysteresis loops for 9% Cr and 12% Cr martensitic steels at a temperature of 500°C.

The influence of a steady bias field on the hysteresis loops of 12Cr-1Mo alloy is illustrated by Fig.10, from which it is seen that the loops diminish in area and approach a straight line, the slope of which decreases with increasing bias field. The area enclosed by the B-H loop represents the so-called hysteresis energy loss incurred in taking unit volume of the material through a complete magnetisation cycle. The observations presented in Fig. 10 thus permit an estimate of the hysteresis energy loss in reactor structures fabricated from HT-9 alloy. This topic is discussed further in section 6.5. Figure 11 shows values of the saturation induction for HT-9 alloy, calculated from the apparent slope of the B vs H characteristic

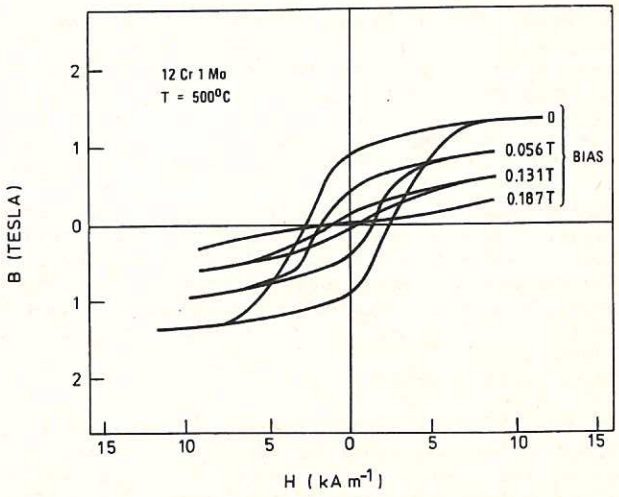

Fig.10 Results from Ref.15 showing the variation of hysteresis loops with bias field for 12Cr 1Mo alloy at 500°C.

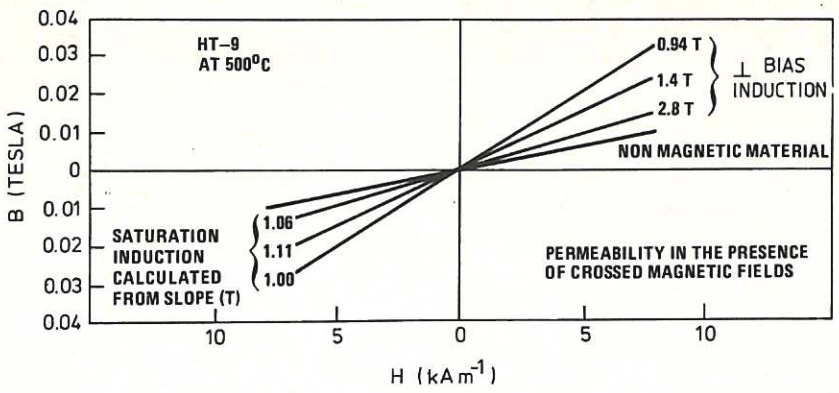

Fig.11 Magnetic properties of HT-9 alloy in simulated tokamak environment (from Ref.15).

Table 12 Saturation induction as a function of temperature for alloys 12Cr-1Mo and 9Cr-2Mo

temperature	25°C		500°C	
alloy	H (kAm^{-1})	B (tesla)	H (kAm^{-1})	B (tesla)
12Cr-1Mo	9.87	1.41	9.71	1.11
9Cr-2Mo	10.6	1.62	10.1	1.33

by an iterative technique designed to correct for the reduction of the bias field within the specimen by demagnetisation. Rawls et al conclude that under reactor conditions, involving a wall temperature around 500°C and a steady toroidal field of about 4T, the saturation flux density of 9-12% Cr martensitic stainless steels is approximately 1.1-1.3 tesla. Thus the effective permeability $(B_o + B_s)/B_o$ with respect to the poloidal field will be less than 1.33. The implications of utilising ferromagnetic first wall/blanket materials will be considered in more detail in subsequent sections, where it will be shown that the effects are relatively minor and can probably be accommodated within the reactor design.

5.2 Investigations by Praeg on 9% Cr steel

Praeg [30] at Argonne National Laboratory has measured the electrical resistivity and magnetic properties of a 9% Cr ferromagnetic steel having the following composition:

Fe	Cr	Mo	Mn	Si	Nb	V	C	P	S
86.2	9.0	2.0	1.0	0.75	0.50	0.30	0.15	0.3	0.3

Observations were made both on rectangular specimens measuring 12.3 x 12.3 x 25.4 mm and on a toroidal sample. B-H curves for the rectangular specimens at room temperature were obtained with a permeameter employing a large electromagnet to generate magnetic fields up to 1.3 MAm^{-1}. These curves are shown in Figures 12 and 13.
(Figs 12 and 13 here)

In Fig. 12 the full curves correspond to a magnetisation axis along the length of the specimen, whilst the dashed curves refer to magnetisation perpendicular to the longitudinal axis. The maximum permeability μ_m, defined here as the gradient of the tangent from the origin to the knee of the curve, is about 400 at B = 1 tesla and at room temperature the steel saturates magnetically below 2 tesla. The difference between the solid and dashed curves in Fig. 12, corresponding to the different orientations of the specimen, is ascribed by Praeg to variations in the length of the air gap relative to the length of the specimen. It seems likely that demagnetisation effects in the sample would also play a significant part.

The toroidal specimen had an outside diameter of 101.6 mm and a rectangular cross section of 11.1 x 11.1 mm. A flux measurement coil consisting of 103 uniformly spaced turns of insulated nichrome wire was wound over the torus and an excitation coil of 354 turns was wound over the flux coil in three

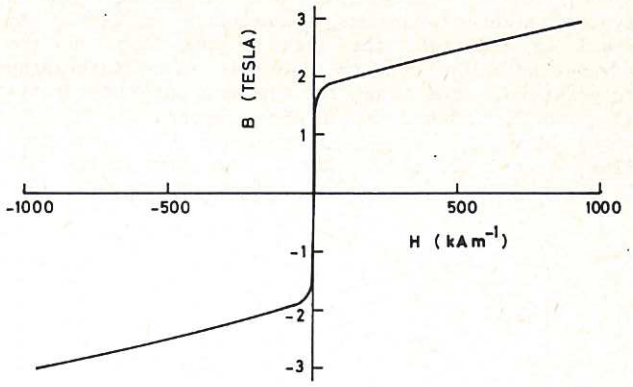

Fig.13 Curve showing DC saturation of the 9%Cr sample.

layers. Provision was made for heating the torus above its Curie temperature. For observation of the basic B-H characteristics the excitation coil was supplied with a sinusoidal current at 0.5 Hz, monitored by means of the voltage developed across a series resistor. A voltage signal proportional to $B = \int B dt$, was obtained by electronic integration of the signal from the flux measurement coil. The magnetisation curve and hysteresis loop for a magnetising field up to 4.4 kAm^{-1} are shown in Fig. 14.

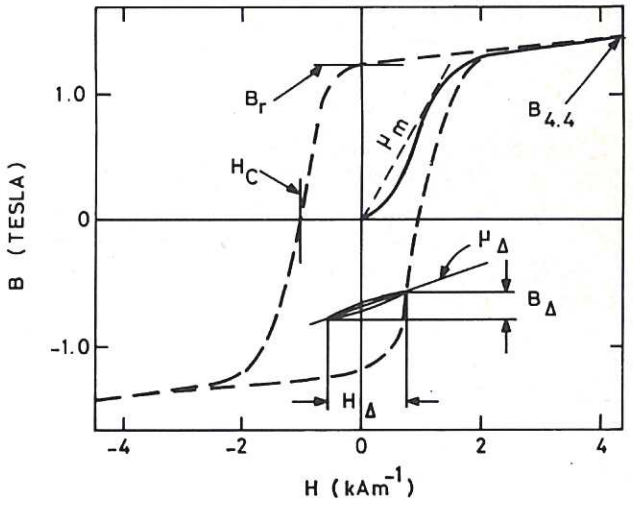

Fig.14 Magnetisation curve (solid line) and hysteresis loop (broken line) for 9%Cr sample in toroidal form with alternating inducing field of amplitude 4.4kAm^{-1} and frequency 0.5Hz.

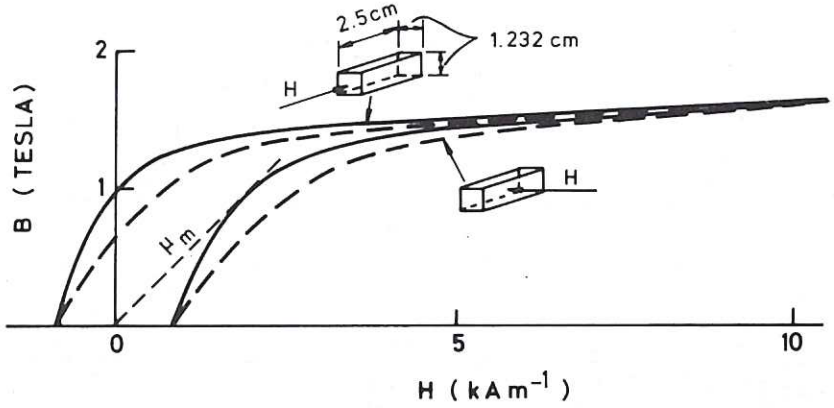

Fig.12 DC hysteresis loops for 9%Cr 2%Mo stainless steel sample for H≤10kAm^{-1} (from Ref.30).

Graphs showing the variation of relative permeability, coercive force and induction with temperature for a sinusoidal excitation field of amplitude 4.4 kAm^{-1} and frequency 0.5 Hz are given in Fig. 15. The Curie point of the sample is seen to be at 705 °C and a maximum permeability $\mu_m = 675$ is attained at about 400°C. The measurements yield $\mu_m \simeq 515$ at 20°C; a value somewhat higher than the $\mu_m \simeq 400$ obtained from the permeameter measurement. The difference is attributed by Praeg to the effect of air gaps which are unavoidable with the permeameter and cause a shearing of the B-H curve. The permeability at H = 4.4 k Am^{-1}, denoted by $\mu_{4.4}$, is also shown in Fig. 15 as a function of temperature.

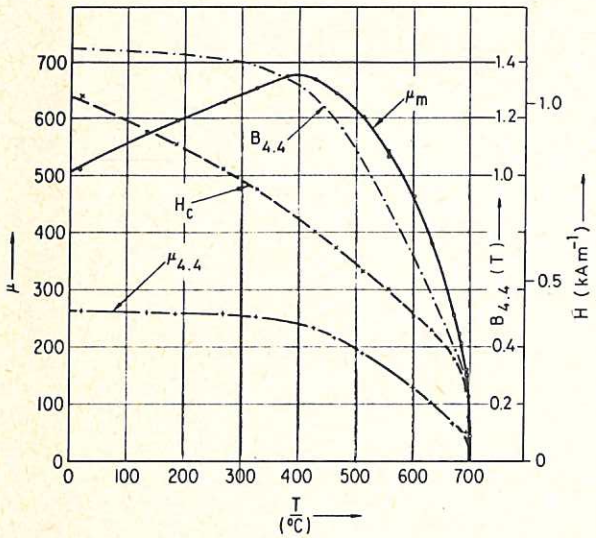

Fig.15 Temperature variations of the AC permeability, coercive force and magnetic induction for 9%Cr steel with alternating inducing field of amplitude 4.4kAm^{-1} and frequency 0.5Hz, according to Ref.30).

The effect of excitation frequency on the hysteresis loop of the toroidal sample is illustrated by Fig. 16. It is evident that at 20°C the loop broadens significantly between f = 0.05 Hz, which represents a close approximation to the DC case, and f = 0.5 Hz, corresponding to the excitation frequency for the measurements described above. These results indicate a DC permeability of about 870, about 70% larger than the value $\mu_m = 515$ measured at f = 0.5 Hz. The dependence of the susceptibility on the measurement frequency is a phenomenon well known in ferromagnetism, though it

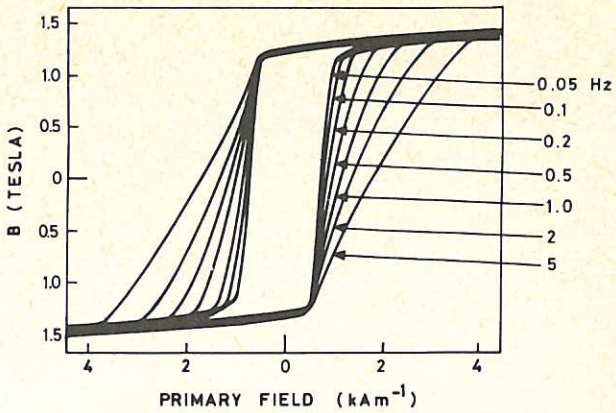

Fig.16 Hysteresis loops for toroidal sample of 9%Cr steel for various frequencies at 20°C.

apparently lacks a simple explanation. The variation of the magnetic properties with frequency probably accounts for the somewhat higher susceptibility values reported by Praeg for 9Cr-2Mo steel in comparison with the values given by Rawls et al, based on measurements at f = 60 Hz. However, the two sets of measurements indicate comparable values of the saturation flux density, which is the magnetic parameter of principal interest in reactor design.

6. INFLUENCE OF FERROMAGNETIC FIRST WALL MATERIAL ON THE REACTOR SYSTEM

6.1 Effect on toroidal field ripple

The influence of a ferromagnetic blanket on toroidal field ripple has been estimated by Chen et al [14] through computations applied to three conceptual tokamak reactor designs denoted by GA TNS, ETF and STARFIRE. Some relevant design parameters for these models are indicated in Table 13.

Since the ambient field exceeds 2 tesla (T) in all three cases, the saturation polarisation in the blanket material was taken as 1T, in accordance with the experimental results described in section 5. Fig.17 shows the outcome of the computations for STARFIRE.

There the midplane toroidal field ripple is plotted as a function of radius for the three cases of (1) a non-magnetic blanket, (2) an asymmetric ferromagnetic blanket, and (3) a ferromagnetic

Table 13
Parameters employed for estimation of forces and field perturbations in the three tokamak models GA TNS, ETF and STARFIRE.

Parameters	GA TNS	ETF	STARFIRE
plasma major radius, R (m)	3.6	5.0	6.92
plasma current (MA)	11.4	5	13.5
number of toroidal field coils	12	12	12
total number of TF ampere turns(10^6A-turns)	90	132	183
toroidal field on axis (T)	5	5.3	5.3
blanket thickness (m)	1	1	1.3
inner blanket inside radius (m)	-	2.8	4.5
inner blanket outside radius (m)	-	3.0	4.9
outer blanket inside radius (m)	4.6	7.1	8.4
outer blanket outside radius (m)	5.6	8.1	9.7

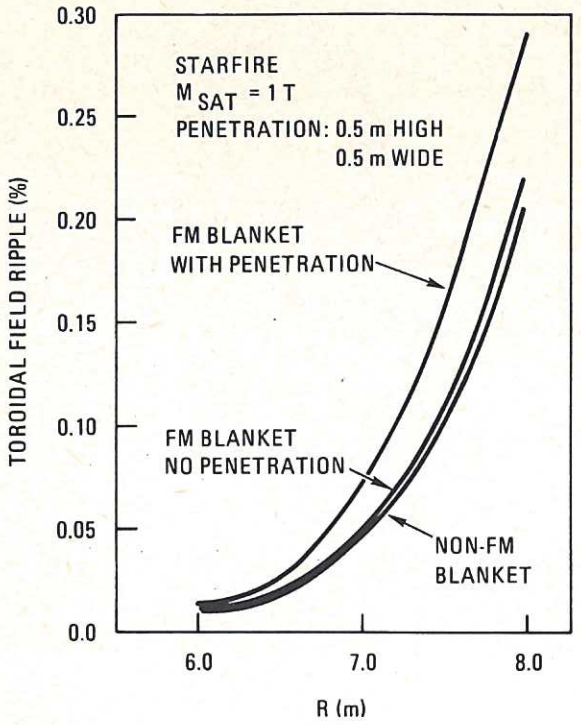

Fig.17 Toroidal field ripple in STARFIRE showing the influence of a ferromagnetic blanket both with and without penetrations.

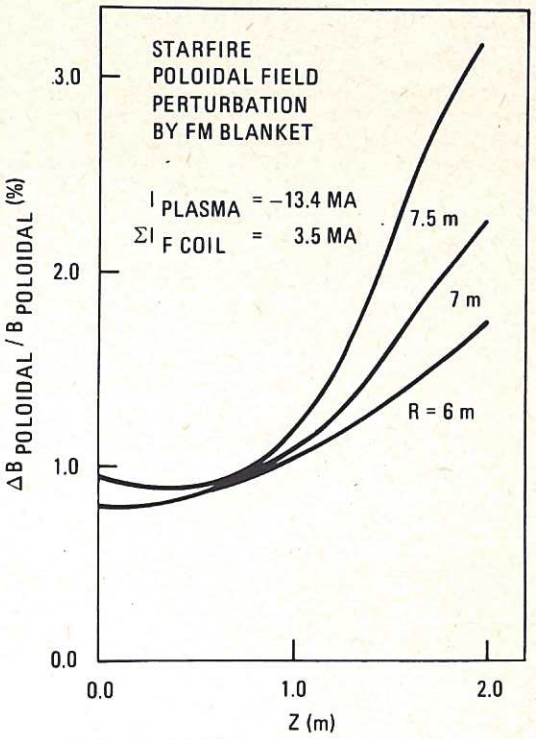

Fig.18 Poloidal field perturbation in STARFIRE caused by a ferromagnetic blanket.

blanket with 0.5 x 0.5m penetration. The axisymmetric ferromagnetic blanket evidently causes only a minor perturbation of the field ripple. In the case with a penetration present the disturbance is larger but still fairly modest over the plasma region.

Chen et al [14] note that similar results were obtained for GA TNS and ETF and conclude that, owing to their state of magnetic saturation, the ferromagnetic blankets have an effective relative permeability close to 1 and do not lead to any significant modification of the toroidal field ripple.

6.2 Effect on poloidal field

Since the toroidal field will normally saturate the blanket region, any ferromagnetic first wall or blanket material will behave in the poloidal field as if it had a relative permeability close to unity. Disturbances in the poloidal field caused by the presence of a ferromagnetic blanket were studied by Rawls et al by comparing the poloidal field distributions for a given poloidal current distribution both with and without the blanket [15]. The results of the computation for STARFIRE are given in Fig.18, which shows the field perturbation as a function of position in the plasma region. It is seen that poloidal field variations up to about 3% can be expected to result from the presence of the ferromagnetic blanket. According to Ref.11, this result should remain valid even if μ is as high as 1.5. A perturbation of this magnitude should not cause major disturbance and could if necessary be counteracted by appropriate programming of the active control system for the poloidal field coils.

6.3 Magnetic forces on the blanket

The effect of weak ferromagnetism in the first wall material of a tokamak reactor has been studied by the General Atomic group [13-15] with the aid of a computer program IRON developed for the solution of non-linear three dimensional magnetostatic field problems. These workers also used an analytical method based on an infinitely long cylinder model. Table 14 indicates the magnitudes of the magnetic forces and the equivalent pressures acting on the blankets corresponding to the three conceptual design models GA TNS, ETF and STARFIRE. The results in the table were derived using the analytical method, which gives values about 20% higher than those from the IRON program.

Figure 19 shows a number of analytically calculated equivalent magnetic pressures as a function of magnetisation multiplied by packing

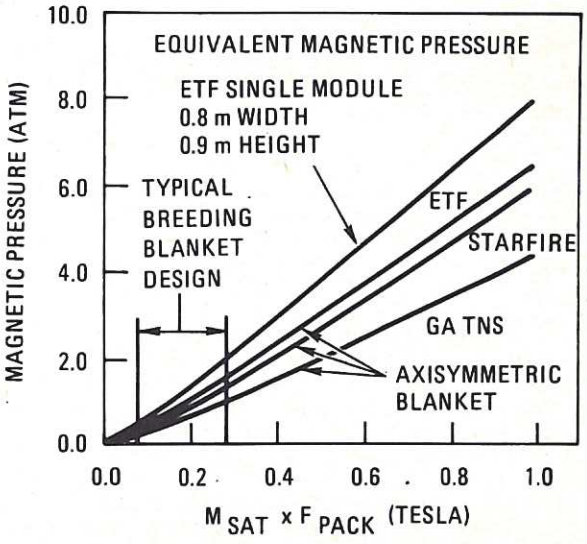

Fig.19 Magnetic loading on the ferromagnetic blankets for the GA TNS, ETF and STARFIRE designs.

Table 14

Radial body forces and equivalent inward pressures calculated by Rawls et al for the three tokamak models GA TNS, ETF and STARFIRE at two values of M, the saturation magnetisation multiplied by the packing factor.

	Design concept					
	GA TNS		ETF		STARFIRE	
major radius (m)	3.6		5.0		6.9	
assumed field on axis (T)	5		5.3		5.3	
	inboard	outboard	inboard	outboard	inboard	outboard
blanket inside radius (m)	-	4.6	2.8	7.1	4.5	8.6
blanket outside radius (m)	-	5.6	3.0	8.1	4.9	9.7
inward pressure (atmospheres)						
for M = 0.5T	-	2.8	2.3	1.9	2.5	2.4
M = 1T	-	6.4	5.1	4.4	5.5	5.3
body force (Mn m^{-3})						
for M = 0.5T	-	0.31	1.3	0.21	0.7	0.2
M = 1T	-	0.7	2.7	0.46	1.5	0.44

factor. This product was chosen as the argument to allow for the fact that only a small proportion of the volume is occupied by magnetic material. The calculations show that the static magnetic pressures amount only to a few atmospheres. Since the additional force on the blanket acts radially inward, towards the major axis, the overall force is a compressive one and it should be feasible to design the blanket modules in such a way that a self-supporting 'keystoned' structure results. Moreover, the magnetic loading on the blanket of an actual fusion reactor might be considerably lower than that indicated by the calculated values, since much of the volume at present assumed to be occupied by ferromagnetic material would probably be taken up by breeding material and coolant flow channels.

The authors of Ref.15 also conclude that the presence of a ferromagnetic blanket would not significantly affect the magnitude of transient loads associated with plasma disruptions.

While the equivalent magnetic pressures appear fairly modest, in comparison with atmospheric pressure for example, they would, in the case of a fusion reactor of economic size, act on large and possibly extended structures. The significance of the additional magnetic forces in relation to other forces such as self-weight and thermal stresses might therefore require a more detailed assessment in the structural design of a reactor incorporating ferromagnetic first wall or blanket materials.

6.4 Transient effects - electromagnetic shielding

In a tokamak device the first wall/blanket must allow penetration of the field from the equilibrium coils, which controls the shape and position of the plasma. The electromagnetic shielding effects of cylindrical structures can be calculated if their electrical resistivity ρ and effective magnetic permeability μ are known.

A rather general consideration of the effects of ferromagnetic blanket materials on transient flux changes has been given by Rawls et al [15]. These authors consider the following processes as being the most significant in relation to tokamak operation:-

1. Ohmic heating by means of rapidly changing currents in an ohmic-heating coil system.
2. Plasma control through controlled current excursions in a set of field control coils.
3. Plasma interruption.

It is assumed that any metallic blanket material, irrespective of its magnetic properties, will need to be subdivided into electrically insulated sections in order to permit ohmic heating by means of an external ohmic-heating coil system. In electrical power engineering the usual aim is to subdivide the conducting material such that the characteristic dimension of the subdivided component, namely the dimension perpendicular to the magnetic flux direction, is of the same order as the skin depth at the operating frequency. The skin depth δ is given by the following well-known relationship[33]:-

$$\delta = \left(\frac{\rho}{\mu\mu_o \pi f}\right)^{\frac{1}{2}}$$

where

ρ = electrical resistivity
μ = magnetic permeability
μ_o = permeability of free space
f^o = equivalent frequency

For HT-9 steel, which has a resistivity $\rho \simeq 1 \times 10^{-6}$ Ωm at 500°C, this equation indicates a skin depth of about 0.3m, assuming a plasma interruption time of 1ms and an effective relative permeability of 1.2. For an austenitic stainless steel such as 316 the skin depth would be essentially the same while for copper it would be about 7mm under the same conditions. Rawls et al modelled the eddy current effects in a cylindrical blanket by means of

two skin coils, one on each surface of the blanket. The effect of any radial cuts in the blanket could be accommodated by specifying a negative number of turns for one of the coils. The reduction of inductance through the skin effect was estimated by integration of a simplified diffusion equation describing the penetration of flux into a magnetic material. These calculations showed that the inductance changes by only a few percent for a ramp time of 1ms. The degree of disturbance depends on the ratio of the cross sectional area of the blanket and the poloidal field flux area within the whole control field coil. A change of about 2% was found for ETF and STARFIRE and about twice as much for GA TNS, which has half as much coil area. Though the calculations of Rawls et al are only approximate they clearly indicate that the field perturbations and time delays involved in penetration of the blanket by control fields are insignificant. Moreover, the magnitude of these disturbances is roughly the same for saturated ferromagnetic materials as it would be for non-magnetic conductors.

Praeg [30] has also considered the problem of electromagnetic shielding and has provided values of the magnetic attenuation factor in convenient graphical form as a function of the relevant parameters.

6.5 Hysteresis energy losses

Energy is dissipated as heat in the material whenever a ferromagnetic material is taken round a hysteresis cycle. This hysteresis loss is to be distinguished from the ordinary eddy current losses which may occur simultaneously. The energy dissipated per unit volume in each cycle is given by the area enclosed within the B vs H hysteresis loop:

$$W = \oint B dH$$

For periodically varying fields the hysteresis loss is proportional to the frequency whereas the eddy current losses, at least for moderately low frequencies, are roughly proportional to the square of the frequency [37]. Figure 20 shows a plot of the hysteresis loss for HT-9 alloy at 500°C as a function of the static bias field. These losses were calculated from the hysteresis curves determined by Rawls et al [15] and shown in Fig. 10 of the present paper.

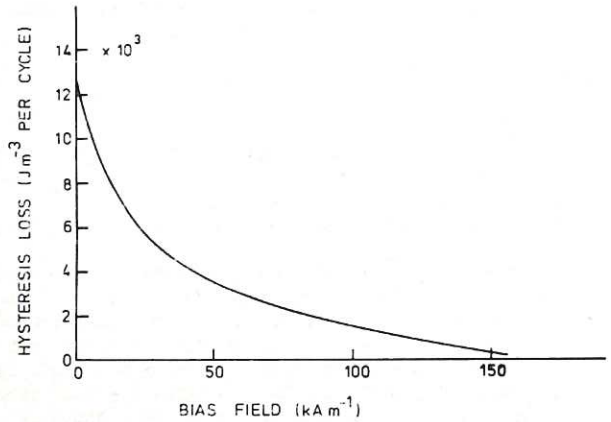

Fig.20 Calculated magnetic hysteresis loss in HT–9 steel at 500°C as a function of static bias field, based on the B–H loops reported by Rawls et al.

The volume of ferromagnetic material in the blanket of a conceptual reactor such as CCTRII could be about 800 m^3 [34]. According to the graph in Fig. 20, the hysteresis energy loss for this volume of HT-9 alloy could be as high as 10^7 joules per cycle in zero bias field, though it would be about three orders of magnitude smaller in the saturating toroidal field. Even in the case of zero field, however, the energy loss per cycle through hysteresis in a ferromagnetic blanket structure is small in comparison with the estimated circulating energy of around 6 GJ associated with neutral injection, refrigeration and the operation of auxiliaries [35].

7. CONCLUSIONS

A number of studies aimed at the assessment of martensitic stainless steels as structural materials in nuclear fusion reactors have recently been published. These studies have included considerations of the mechanical properties, the effects of irradiation, neutron activation and the implications of a ferromagnetic susceptibility. It appears that certain martensitic stainless steels containing 9-12% Cr may offer the potential of a longer lifetime than some of the present candidate materials, e.g. type 316 austenitic steel. Considerations of induced radioactivity, afterheat and future resource availability also appear to favour alloys of the martensitic group in preference to the austenitic grades.

The weak ferromagnetism exhibited by stainless steels of the ferritic/martensitic groups has hitherto been regarded as a potentially serious drawback to their application in magnetic confinement fusion devices. The first wall/blanket material in a tokamak device will be magnetically saturated by the toroidal field, however, and the studies performed by the General Atomic Group indicate that its effect on the toroidal field ripple, on transient field variations and on the field-shaping coils will be insignificant. The additional magnetic forces on the blanket are directed toward the major axis and are equivalent to a static pressure not exceeding a few atmospheres. It seems likely that this additional pressure could be accommodated within the mechanical design of a reactor, though more detailed calculations applied to specific models may be needed to confirm this conclusion. The ferromagnetism of the martensitic alloys is thus not expected to pose any serious system design problems.

Further work will be needed to establish the applicability of martensitic stainless steels as structural materials in fusion reactors and the following subject areas appear to require further study:-

1. Influence of the fusion reactor environment on structural properties, in particular the effect of neutron irradiation to the levels of dpa and the ratios of hydrogen and helium concentrations to dpa appropriate to fusion reactor conditions.
2. Further investigation of the change of fracture toughness at lower temperature associated with the ductile-to-brittle transition.
3. Weldability and fabricability - in particular the optimum pre- and postweld heat treatment, susceptibility to cracking, development of repair procedures and the sensitivity of welding procedures to microstructure.

8. GENERAL BIBLIOGRAPHY

E.C. Rollason, Metallurgy for Engineers, 4th ed. Edward Arnold, London 1973.

J.H.G. Moneypenny, Stainless Steels, Chapman and Hall.
Metals Handbook, 8th ed. Amer. Soc. Metals.
Smithells, Metals Reference Book, 3rd ed. Butterworths 1962.
F.B. Pickering, Physical Metallurgy and the Design of Steels, Applied Science Publishers, 1978
D. Peckner and I.M. Bernstein, Handbook of Stainless Steels, McGraw Hill, N.Y., 1977.
Metals Properties, A.S.M.E. Handbook, McGraw Hill.
Handbooks on Armco Stainless Steels, Armco Steel Corp., Middletown, Ohio.
Republic Enduro Stainless Steels, Republic Steel Corp., Cleveland, Ohio.
Radiation Damage in Metals ed. N.L. Peterson and S.D. Harkness, Amer. Soc. Metals 1976.
R.W. Conn, First wall and diverter plate material selection in fusion reactors, UWFDM - 237, 1978.
The fusion reactor materials, section IV, DOE/ET-0032/4 1978.
The Super 12% Cr Steels, Climax Molybdenum Company 1965.
C.T. Sims and W.C. Hagel, The Superalloys, Interscience 1973.
R.M. Brick, R.B. Gordon and A. Philips, Structure and Properties of Alloys, McGraw Hill, NY, 1965.
L.H. Van Vlack, A textbook of Materials Technology, Addison Wesley, 1973.

9. REFERENCES

1. D.L. Smith, R.G. Clemmer, S.D. Harkness, J. Jung, J.L. Krazinski, R.F. Mattas, H.C. Stevens, C.K. Youngdahl, C. Trachsel, D. Bowers, B. Cramer, J. Davis, G. Fuller and D. Morgan, Fusion reactor blanket/shield design study, ANL/FPP-79-1.
2. Metals Handbook 8th ed., American Society for Metals, Metals Park, Ohio, 1961.
3. D. Peckner and I.M. Bernstein, Handbook of stainless steels, McGraw Hill, N.Y. 1977.
4. F.B. Pickering, Physical metallurgy of stainless steel developments, International Metal Reviews, Dec. 1976, 227.
5. E. Baerlecken, W.A. Fischer and K. Larenz, Studies of the transformation behaviour, the notch impact toughness and the tendency toward intercrystalline corrosion in iron-chromium alloys with chromium contents up to 30%, Stahl Eisen 81, 768 (1961).
6. H. Schneider, Foundry Trade J. 108, 562 (1960).
7. J.J. Demo, Structure and constitution of wrought ferritic stainless steels, Ch. 5 of Handbook of Stainless Steels, ed. D. Peckner and I.M. Bernstein, McGraw Hill, NY, 1977
8. E.A. Little, D.R. Harries, F.B. Pickering and S.R. Keown, Effects of heat treatment on structure and properties of 12% Cr steels, Metals Technology, 4, 205 (1977)
9. E.A. Little, D.R. Harries and F.B. Pickering, Some aspects of the structure-property relationship in 12% Cr steels, Proc. BNES Conf. on ferritic steels for fast reactor steam generators, London May/June 1977, eds. S.F. Pugh and E.A. Little 1, 136 (1978)
10 C.J. Novak, Structure and constitution of wrought austenitic stainless steels, Ch. 4 of Handbook of Stainless Steels, ed. D. Peckner and I.M. Bernstein, McGraw Hill, NY, 1977
11. INTOR - International Tokamak Reactor, Final Report, I.A.E.A., Vienna.
12. R.F. Mattas, Austenitic stainless steel bulk property considerations for fusion reactors, ANL/FPP/TM-86.
13. S.N. Rosenwasser, P. Miller, J.A. Dalessandro, J.M. Rawls, W.E. Toffolo and W. Chen, The application of martensitic stainless steels in long lifetime fusion first wall/blankets, GA-A15356 1979.
14. W.Y. Chen, U.A. Peuron, P.H. Miller, J.M. Rawls and S.N. Rosenwasser, Magnetics aspects of martensitic stainless steels as structural materials for tokamak reactors, GA-A15619 1979.
15. J.M. Rawls, W.Y.K. Chen, E.T. Cheng, J.A. Dalessandro, P.H. Miller, S.N. Rosenwasser and L.D. Thompson, Assessment of martensitic steels as structural materials in magnetic fusion devices, GA-A15749 1980.
16. L.M. Wyatt, The performance of Cr-Mo steels in the boilers of CEGB power stations in 'Ferritic steels for fast reactor steam generators', Ed. S.F. Pugh and E.A. Little (1978), Proc. Int. Conf. of British Nuclear Energy Society, London, 1977.
17. F.A. Smidt, P.R. Malmberg, J.A. Sprague and J.G. Westmoreland, Swelling behaviour of commercial ferritic alloys EM-12 and HT-9 as assessed by heavy ion bombardment, in 'Irradiation effects on the microstructure and properties of metals', ASTM STP no. 611, Amer. Soc. for Testing and Materials (1976).
18. J.C. Spanner, Ed. Nuclear Systems Materials Handbook, Vol. 1 Design Data.
19. J.I. Bramman et al, Void swelling and microstructural changes in fuel pin cladding and unstressed specimens irradiated in DFR, Proc. Int. Conf. on radiation effects in breeder reactor structural materials, Scottsdale, 1977, AIME, 1977, p479
20. E.A. Little, Void swelling in irons and ferritic steels Part 1: Mechanisms of swelling suppression, J. Nucl. Materials 87, 11 (1979)
21. E.A. Little and D.A. Stow, Void swelling in irons and ferritic steels Part II: an experimental survey of materials irradiated in a fast reactor, ibid p25
22. E.A. Little et al; Proc. Int. Conf. on irradiation behaviour of metallic materials for fast reactor core components, Ajaccio, Corsica, 1979 p31
23. E.A. Little and D.A. Stow, ibid p17
24. E.A. Little, R. Bullough and M.H. Wood, On the swelling resistance of ferritic steel, Proc. Roy. Soc. A372, 565 (1980)
25. K. Anderko, Zur Eignung warmfester Vergutungsstahle mit 9 bis 12% chrom fur Komponenten im kern schneller Reaktoren - ein Uberblick, J. Nucl. Materials, 95, 31 (1980)
26 F.A. Smidt, J.R. Hawthorne and V. Provenzano, The fracture resistance of HT-9 after irradiation at elevated temperature, Proc. Symposium on Effects of Radiation on Structural Materials, Georgia, June 1980
27. T.Y. Sung and F. Vogelsang, DKR: a radioactivity calculation code for fusion reactors, Report No. UWFDM-170, Nuclear Engineering Dept., University of Wisconsin 1976
28. Ceramic materials for fusion reactors, Electric Power Research Institute Report, EPRI AP-1499, 1980
29. T.Y. Sung, Radioactivity calculation in fusion reactors, PhD thesis, University of Wisconsin, 1976
30. W. Praeg, Magnetisation hysteresis and eddy current shielding of 9% Cr stainless steel as a function of temperature, 8th Symp. on Eng. Problems of Fusion Research, San Francisco, Nov. 1979.
31. C.D. Graham, Method for measuring saturation magnetisation in ring samples, J. Appl. Phys. 29, 68 (1958)
32. H. Zijlstra, Experimental methods in magnetism 2. Measurement of magnetic quantities, North Holland 1967 p136
33. W.R. Smythe, Static and Dynamic Electricity,

3rd ed, p.370, McGraw Hill, N.Y. 1968
34. D.A. Briaris and J.R. Stanbridge, Design of the segment structure and coolant ducts for a fusion reactor blanket and shield, Culham Laboratory Report CLM-R184 (1978)
35. W.R. Spears and R. Hancox, A pulsed tokamak reactor study, Culham Laboratory Report, CLM-R197 (1979)
36. G.W.C. Kaye and T.H. Laby, Tables of Physical and Chemical Constants, 14th ed, Longman, London, 1973
37. R.M. Bozorth, Ferromagnetism, Van Nostrand, N.Y., 1959

Appendix A

The AISI classification system for stainless steels

The American Iron and Steel Institute (AISI) jointly with the Society of Automotive Engineers (SAE) has devised a widely recognised number code for the classification and description of steel alloys. For stainless steels the AISI system employs a three-digit code in which the first digit defines a major series, the following two digits identify the particular grade and, where used, a letter suffix represents a modification of that grade. The major series are as follows:

200 Series	Iron-chromium-nickel-manganese alloys - nonhardenable, austenitic
300 Series	Iron-chromium-nickel alloys - non-hardenable, austenitic
400 Series	Iron-chromium alloys - hardenable or non-hardenable, martensitic or ferritic, depending on carbon or nitrogen content
500 Series	Low-chromium iron alloys - heat resistant, non-stainless

The major categories comprise the 300 series nickel-stabilised austenitic alloys and the 400 Series alloys which are either nickel free or have nickel content below 2.5%. The 200 Series represents austenitic alloys in which a proportion of the nickel content has been replaced by manganese and nitrogen whilst the 500 Series comprises steels containing 4-6% Cr. The suffix letter L, e.g. type 304L, generally denotes a modification having low carbon content, a low nitrogen content being similarly indicated by the suffix LN.

Hardenability is not confined to alloys of the martensitic group since work hardening, precipitation hardening and sigma hardening can occur in austenitic and ferritic alloys. Moreover, martensite, ferrite and austenite may be present to some extent in steels of all groups and, in practice, these terms are often used in a rather imprecise sense to distinguish between classes of steels on the basis of their behaviour under heat treatment.

Appendix B

A review of basic concepts and definitions in ferromagnetism

So far as their magnetic properties at normal temperatures are concerned nearly all materials can be classified into two major groups. The members of one group, made up of diamagnetic and paramagnetic substances, are only weakly magnetic. In these materials the intensity of magnetisation induced by an applied field lies in the direction of the field and is proportional to it. A medium of this kind which is uniform and without intrinsic directional properties is said to be linear, homogeneous and isotropic. For these materials the magnetic moment per unit volume, J, and the magnetic induction B are proportional to the applied field H. The correlation between B and H can be expressed by the equation

$$B = \mu\mu_o H$$

in which μ is a dimensionless factor of proportionality known as the relative permeability and μ_o is a constant with numerical value $4\pi \times 10^{-7}$ henries.m^{-1}, termed the permeability of free space. The value of μ varies with the material.

Paramagnetic and diamagnetic substances have permeabilities which differ only slightly from unity and these materials are more conveniently described by the volume susceptibility κ defined by the relation

$$\mu = \mu_o (1 + \kappa)$$

or, alternatively, by the mass susceptibility χ, equal to the volume susceptibility divided by the density of the material, ρ

$$\chi = \frac{\kappa}{\rho}$$

In SI units the magnetic properties are described in terms of the magnetic field strength H (ampere per metre), flux density B (tesla, T) and magnetic polarisation J, with the corresponding relations:

$$B = \mu\mu_o H$$
$$= \mu_o H + J$$
$$\mu = \mu_o (1 + \kappa)$$

The relative permeability $\mu_r = \mu/\mu_o$ is the permeability of the material relative to that of free space.

The other group, comprising the ferromagnetic materials, principally iron, nickel, cobalt and related alloys, is strongly magnetic and non linear. The magnetic behaviour of members of this group is, moreover, dependent on the mechanical, thermal and magnetic history of the sample. The relation between B and H is not a simple one but is double-valued and the relative permeability, which is generally much larger than unity, is no longer a constant but depends on H and on the previous magnetic history of the specimen. Some typical values of diamagnetic and paramagnetic susceptibilities and ferromagnetic permeabilities are given in Table 15, based on data taken from Kaye and Laby[36]

The behaviour of a ferromagnet is usually described by its B vs H and μ vs H curves. Considering an initially unmagnetised sample in the form of a torus, which eliminates demagnetisation effects, the magnetisation induced by an applied field along the minor axis of the toroid is obtained

Table 15

Susceptibilities of some common diamagnetic and paramagnetic substances and permeabilities of some typical ferromagnetic materials

SUBSTANCE	SUSCEPTIBILITY per kg at 20°C (values to be multiplied by 10^{-8})	
Diamagnetic materials		
Hydrogen	- 2.5	
Copper	- 0.107	
Lead	- 0.15	
Water	- 0.90	
Sodium chloride	- 0.64	
Paramagnetic materials		
Oxygen	+ 134	
Aluminium	+ 0.82	
Sodium	+ 0.75	
$CuSO_4.5H_2O$	+ 7.7	
$MnSO_4.4H_2O$	+ 81.2	
Ferromagnetic materials		
	Relative permeability μ_r	
	Initial	Maximum
Armco iron (99% Fe)	250	7000
Silicon-iron, dynamo grade	1000	6000
Mumetal	$\sim 5 \times 10^4$	$\sim 10^5$
Type A Mn-Zn ferrite	~ 1000	~ 3000
18-8 stainless steel, austenitised	1.005 - 1.03	
18-8 stainless, 20% cold reduction	1.4	
Hadfields Mn steel	1.03	
Clyde alloy non-magnetic steel	1.003	

by plotting the intensity of magnetisation M or the magnetic induction B against the field strength H. The material initially follows a curve similar to the solid line oa in Fig. 21.

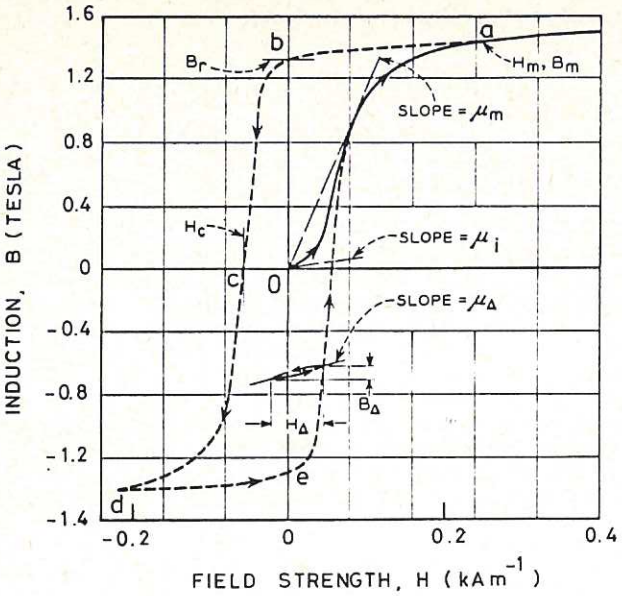

Fig.21 B versus H for a typical ferromagnetic material.

The slope of the tangent to the curve oa at the origin is known as the initial permeability, μ_i. As H is increased indefinitely the intensity of magnetisation M and the intrinsic induction (B - H) of the specimen approach a definite limit B_s which represents a state of magnetic saturation. The induction B increases indefinitely, however, owing to the increasing contribution of H to the flux density. On reducing the applied field the curve ab is obtained. With zero field at point b, the sample still retains a substantial residual induction ob (if the field has been sufficient to attain saturation this is referred to as the retentivity) which provides a measure of its ability to retain magnetism when not subjected to adverse treatment. Application of an increasing field in the reverse direction results in the curve bcd. At point c the demagnetising field of magnitude oc causes complete loss of the magnetisation previously acquired in the field at point a. The field oc is termed the coercive force (or coercivity, if the saturation induction was attained) and represents the ability to retain magnetism in spite of adverse treatment. Reduction of the field gives the branch de, while reversing and increasing it again gives ea. The magnetisation always lags behind the applied field - an effect known as hysteresis. The hysteresis loop should be symmetrical about o although several complete cycles may be needed to establish a steady cyclic state. With ferromagnetic materials the permeability can be defined and measured in various ways. The initial permeability μ_i has already been defined. The maximum permeability μ_m is the highest value of normal permeability obtained by varying the amplitude of H and corresponds to the gradient of the straight line from the origin to the knee of the magnetisation curve.

Suppose the specimen is being taken through a magnetisation cycle and that a point is reached on oa or ea. If, instead of proceeding to higher fields, H is reduced by a small amount ΔH, then the magnetisation will fall by a small amount ΔM and the induction by ΔB. If these increments are small enough they are reversible and unaccompanied by hysteresis. In this case the ratio $\Delta B/\Delta H$ is known as the reversible permeability at the point P.

If the specimen is subjected to a steady field upon which an alternating field is superimposed, then an unsymmetrical hysteresis cycle will be described. The ratio of the difference between the extreme values of B and the difference between the extreme values of H is termed the incremental permeability $\mu_\Delta = B_\Delta/H_\Delta$. This parameter reduces to the reversible permeability as $H_\Delta \to 0$.

Hysteresis energy loss

It is readily shown [37] that the area enclosed by the hysteresis loop is proportional to the energy dissipated in taking unit volume of the material through a complete cycle, i.e.

$$W = \oint_{H_1}^{H_1} H dM \quad \text{per unit volume}$$

$$= \oint H dB$$

This energy loss should be distinguished from the ordinary eddy current losses that occur in conducting ferromagnetic materials subjected to time-varying fields. A relationship sometimes useful for estimating the hysteresis loss was discovered empirically by Steinmetz:

$$W = \eta B_{max}^{n}$$

where η is a constant depending on the material and known as the Steinmetz coefficient, and n is a constant of approximate value 1.6.

Effect of eddy currents

Changes of magnetic flux within a conducting medium give rise to electromotive forces and associated electrical currents within the material. These eddy currents depend on the geometry of the material, on its resistivity and permeability and on the rate of change of the flux. The eddy currents flow in such a direction as to oppose the change in flux and thus exert a shielding effect which prevents immediate penetration of the field into the interior of the material. Thus the magnetic induction toward the interior will generally be lower than and will lag behind the value at the surface. The effects associated with eddy currents have been described quantitatively by Bozorth [37] and by Smythe [33] and these references should be consulted for a fuller discussion of the subject.

Interconversion of units

	cgs system	rationalised Mks	SI
Field strength H	$\frac{4\pi}{1000} = 0.01256$ oersted	= 1 ampere-turn m^{-1}	= 1 ampere m^{-1}
Magnetic induction or flux density B	10^4 gauss	= 1 weber m^{-2}	= 1 Tesla

HER MAJESTY'S STATIONERY OFFICE

Government Bookshops

49 High Holborn, London WC1V 6HB
13a Castle Street, Edinburgh EH2 3AR
41 The Hayes, Cardiff CF1 1JW
Brazennose Street, Manchester M60 8AS
Wine Street, Bristol BS1 2BQ
258 Broad Street, Birmingham B1 2HE
80 Chichester Street, Belfast BT1 4JY

Government publications are also available through booksellers